Jestr

Journal of Engineering Science and Technology Review 11 (1) (2018) 208 - 215

Research Article

JOURNAL OF
Engineering Science and Technology Review

www.jestr.org

Optimized Method for Selecting Common Master Image in PS-DINSAR

Xiangtong Liu[1,2,3,*], Qiuxiang Cao[2], Shengping Wang[2] and Chernyatyeva Anastasia[4]

[1] *School of Geoscience and Info-Physics Engineering, Central South University, Changsha 410083, China*
[2] *Department of Geomatics, East China University of Technology, Nanchang 330013, China*
[3] *Key Laboratory for Digital Land and Resources of Jiangxi Province East China University of Technology, Nanchang 330013, China*
[4] *Department of Geology, St. Petersburg State University, St. Petersburg 48202, Russia*

Received 19 October 2017; Accepted 23 January 2018

Abstract

The differential synthetic aperture radar interferometry technique of permanent scatterers (PS-DINSAR) is an important method in the phase analysis of synthetic aperture radar data. Selection of common master image in PS-DINSAR widely influences the data processing results. Most of existing selection methods of common master image are based the statistical characteristics on the baseline of the interferogram and thus cannot ensure best selected results. A method based on fixed weights of observed values in the surveying adjustment was used in this study to extract an optimum image. The temporal baselines, effective spatial baselines, and Doppler centroid frequency difference of image pairs were incorporated in this technique. The sum of normalized weights model was utilized based on integrated correlation coefficient algorithm and minimum sum of three baseline algorithm to obtain optimal common master image. Then, the procedure of selecting common master images based on the idea of maximum sum of normalized weights was introduced and used to test the selection of common master image by using 19 images of ERS-1/2. Result shows that, in comparison with data generated separately by integrated correlation coefficient algorithm and minimum sum of three baseline algorithm, the outcome produced by maximum sum of normalized weights model in this study exhibits considerably better statistical property in temporal baselines, effective spatial baselines, and Doppler centroid frequency difference of image pairs. Moreover, the interferograms show that the maximum, average, and standard deviation values are less than those of others in temporal baselines, effective spatial baselines, and Doppler centroid frequency difference. Therefore, the selected common master is robust and stable. This study provides an effective method for the optimization of common master image and presents certain guiding significance for selecting common master image.

Keywords: permanent scatter DINSAR; common master image; optimum selection

1. Introduction

As the number of synthetic aperture radar (SAR) sensors increases, the application range of SAR data expands, thereby arousing various SAR data processing methods. The differential synthetic aperture radar interferometry technique of permanent scatterers (PS-DINSAR) was first developed in 2000 by Ferretti[1, 2] to overcome the effects of temporal and spatial decorrelation in traditional DINSAR technologies and obtain information of a long time series surface deformation. The idea has attracted attention since its introduction. PS-DINSAR can obtain high coherent points by natural and artificial objects with surface scattering properties and observe surface deformation with properties of high precision and large scale in a long time[3-12].

A single common master image is utilized in PS-DINSAR to generate interferograms. Ferretti selected a common master image by using temporal baselines as reference because this technique can decrease temporal decorrelation. Hopper[13] used the method of shortest temporal baselines and suggested the use of the most middle scene in the image time series as common master image. Kampes[14] continued to study the selection of common master image. However, the complexity in interferograms brings difficulty for existing methods in selecting the optimal common master image[13, 15, 16].

In this study, an idea based on fixed weights of observed values in the surveying adjustment was used to obtain the optimal common master image and thus obtain interferogram sequence of superior quality.

2. State of the art

Selection of common master image is an important step in the PS-DINSAR technology. The selected methods and the evaluation index of the selected results are researched by different scholars. The selection of the common master image under constraint condition with temporal baselines was first used by Ferretti[2]. This way is simple and ignores the consequences of other factors. Hopper[13] adopted the technique of shortest temporal baselines and proposed the use of the most middle scene in the image time series as common master image. Temporal and effective spatial baselines were considered by Kampes[14] to improve the selection of common master image and increase accuracy. However, the possibilities of other factors were ignored. Further relevant research based on this method has been

*E-mail address: tomcleck@126.com
ISSN: 1791-2377
doi:10.25103/jestr.111.25

conducted[17]. Zebker[18] investigated the reasons and influencing factors of InSAR measurement and gained the main causes (i.e., temporal baseline, effective spatial baseline, Doppler centroid frequency difference, and thermal noise), which should be considered in the selection of images. Thus, temporal and effective spatial baselines were used as the selection methods of common master image by Zhang et al.[19]. The influences of the Doppler centroid frequency difference and terrestrial vegetation change at different times in common master image were also analyzed. Chen et al.[20] used composite coefficient of correlation to select common master image. Temporal baseline, effective spatial baseline, and Doppler centroid frequency difference were simultaneously considered in this model. The selection of common master image was determined by the maximum correlation coefficient, which can be used to decide on the optimum images. The minimum sum of baselines was used by Tao et al.[15] to improve optimization efficiency. Nevertheless, the analysis of baseline in the algorithm was extremely simple because the rights of the individual effects of baseline weight were ignored. Wang et al.[21] adopted the method of equal influence to measure the impact of various factors. This technique is stable when data quality is satisfactory; however, it is unsuitable to individual data of poor quality. Luo[22] and Pan et al.[23] used image clustering and orthogonal characteristics to select common master image from the mathematical perspective. Liu[24] mapped all the elements into three-dimensional space and selected the common master image through the location of the space centroid. The two approaches can determine common master image with definite physical properties. However, the process is complex, and the unique features of the interferograms are ignored. Long[25] utilized a priori information of external global position system (GPS) data to select the common master image; however, GPS data are not always available.

In view of the combined effects of various factors, the idea based on observed value fixed weight in surveying adjustment is used in this study to obtain suitable combination for determining the common master image. An improved selection method of common master image by giving the weight to each group is used to select the optimized of combination baseline. The experimental data prove that the algorithm is highly efficient.

The remainder of this study is organized as follows. The basic concepts of surveying error and weight are described in Section 3. The procedure of selecting the common master image by using the maximum sum of weight algorithm is also provided. An application example of the maximum sum of weight is introduced in Section 4. The statistical characteristics of the common master image selected by this technique are also analyzed. The conclusions are drawn in Section 5.

3. Methodology

3.1 Root mean square error (RMSE) and weight

In the surveying adjustment theory, RMSE is an absolute numerical characteristic of accuracy. Definite RMSE occurs when certain observing conditions are relative with error distributions. Given the characteristics of the interferogram results, the interferogram combination is evaluated using the RMSE.

For comparing the accuracy between various observations, the precision of observed values is determined by a proportional relationship between RMSEs. The digital signature that represents the proportional relationship of each observation variance is called weight, that is, a relative numerical characteristic to represent accuracy. Weight plays an important role in the surveying adjustment calculation.

For a group of equal-precision observation:

$$P = \frac{\sigma_0^2}{\sigma_i^2} \tag{1}$$

where P is the weight of an observed value, σ_0^2 is the square of RMSE in unit weight, and σ_i^2 is the square of the RMSE of an observed value.

For such accuracy of the n independent observations (X_1,K ,X_n), the formula of the error in the observations is expressed as follows:

$$m_i = \sqrt{\frac{\sum_{i=1}^{n}\left(X_i - \bar{X}\right)^2}{n-1}} \tag{2}$$

where m_i is the RMSE of the observed value, and $\bar{X}$ is the mean of the observed value (X_1,K ,X_n).

By weighting the observations of each group, the quality of the interferogram sequences can be clearly evaluated.

3.2 Maximum sum of weight algorithm and calculation process

The temporal baseline, effective spatial baseline, and Doppler centroid frequency difference are regarded as independent equal-precision observation groups. The weight of each image combination is solved. The sum of weights is added with the independent value of three weights and is used as the basis of the selection of the common master image. This method is the maximum sum of weights. N interferometricpairs are consisted comprise n images, which include a pair composed by the image and itself. When the ith image is selected as the common master image, the sum of weights is determined as follows:

1) The sequence of observations is composed by the common master image with ith image, and the RMSE of temporal baseline, effective space baseline, and Doppler centroid frequency difference are separately calculated as follows:

$$m_{Ti} = \sqrt{\frac{\sum_{i=1}^{n}\left(T_i - \bar{T}\right)^2}{n-1}} \tag{3}$$

where m_{Ti} is the RMSE of temporal baseline, T_i is the temporal baseline, $\bar{T}$ is the mean of the temporal baseline, and n is the number of image pairs;

$$m_{Bi} = \sqrt{\frac{\sum_{i=1}^{n}\left(B_i - \bar{B}\right)^2}{n-1}} \tag{4}$$

where m_{Bi} is the RMSE of effective spatial baseline, B_i is the effective spatial baseline, $\bar{B}$ is the mean of the effective spatial baseline, and n is the number of image pairs;

$$m_{Di} = \sqrt{\frac{\sum_{i=1}^{n}\left(D_i - \overline{D}\right)^2}{n-1}} \tag{5}$$

where m_{Di} is the RMSE of Doppler centroid frequency difference, D_i is the Doppler centroid frequency difference, $\overline{D}$ is the mean of Doppler centroid frequency difference, and n is the number of image pairs.

2) The weight of RMSE by an observed sequence of the common master image with ith image can be performed alone using the numerical results of m_{Ti}, m_{Bi}, and m_{Di}. The weights of m_{Ti}, m_{Bi}, and m_{Di} can be obtained as follows:

$$P_{Ti} = \frac{m_{T0}^2}{m_{Ti}^2} \tag{6}$$

where P_{Ti} is the weight of m_{T_i}, m_{T_0} is the RMSE of the temporal baseline in unit weight, and m_{T_i} is the RMSE of the temporal baseline;

$$P_{Bi} = \frac{m_{B_0}^2}{m_{Bi}^2} \tag{7}$$

where P_{Bi} is the weight of m_{B_i}, m_{B_0} is the RMSE of the effective spatial baseline in unit weight, and m_{B_i} is the RMSE of the effective spatial baseline;

$$P_{Di} = \frac{m_{D_0}^2}{m_{Di}^2} \tag{8}$$

where P_{Di} is the weight of m_{D_i}, m_{D_0} is the RMSE of the Doppler centroid frequency difference in unit weight, and m_{D_i} is the RMSE of the Doppler centroid frequency difference.

3) The sum of weights of an observed sequence of the common master image with ith image can be determined as follows:

$$P_i = P_{T_i} + P_{D_i} + P_{B_i} \tag{9}$$

where P_{T_i}, P_{D_i}, and P_{B_i} are the weights of m_{T_i}, m_{D_0}, and m_{B_i}, respectively; and P_i is the sum of weights of the observed sequence of the common master image with ith image.

The flowchart shown in Figure 1 depicts the process of calculation.

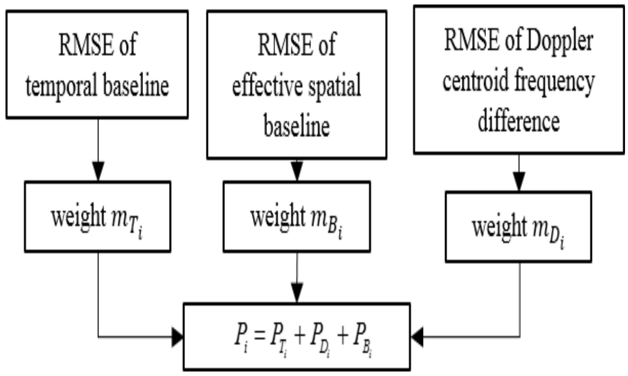

Fig. 1. Flowchart for computing the maximum sum of weights

4. Result analysis and discussion

A total of 19 single look complex images (SLCs) from European Remote Sensing Satellite (ERS-1/2) SAR sensor were acquired as examples (data from Tao[15]) to study the maximum sum of weights and the results of the selection method.

Table. 1. Temporal baseline statistics of interferograms (unit: day)

image	1	2	3	4	5	6	7	8	9	10	11	12	13	14	15	16	17	18	19
1	0	35	70	140	315	350	490	700	804	805	909	910	1085	1120	1190	1400	1470	1645	1715
2	-35	0	35	105	280	315	455	665	769	770	874	875	1050	1085	1155	1365	1435	1610	1680
3	-70	-35	0	70	245	280	420	630	734	735	839	840	1015	1050	1120	1330	1400	1575	1645
4	-140	-105	-70	0	175	210	350	560	664	665	769	770	945	980	1050	1260	1330	1050	1575
5	-315	-280	-245	-175	0	35	175	385	489	490	594	595	770	805	875	1085	1155	1330	1400
6	-350	-315	-280	-210	-35	0	140	350	454	455	559	560	735	770	840	1050	1120	1295	1365
7	-490	-455	-420	-350	-175	-140	0	210	314	315	419	420	595	630	700	910	980	1155	1225
8	-700	-665	-630	-560	-385	-350	-210	0	104	105	209	210	385	420	490	700	770	945	1015
9	-804	-769	-734	-664	-489	-454	-314	-104	0	1	105	106	281	316	386	596	666	841	911
10	-805	-770	-735	-665	-490	-455	-315	-105	-1	0	104	105	280	315	385	595	665	840	910
11	-909	-874	-839	-769	-594	-559	-419	-209	-105	-104	0	1	176	211	281	491	561	736	806
12	-910	-875	-840	-770	-595	-560	-420	-210	-106	-105	-1	0	175	210	280	490	560	735	805
13	-1085	-1050	-1015	-945	-770	-735	-595	-385	-281	-280	-176	-175	0	35	105	315	385	560	630
14	-1120	-1085	-1050	-980	-805	-770	-630	-420	-316	-315	-211	-210	-35	0	70	280	350	525	595
15	-1190	-1155	-1120	-1050	-875	-840	-700	-490	-386	-385	-281	-280	-105	70	0	210	280	455	525
16	-1400	-1365	-1330	-1260	-1085	-1050	-910	-700	-596	-595	-491	-490	-315	-280	-210	0	70	245	315
17	-1470	-1435	-1400	-1330	-1155	-1120	-980	-770	-666	-665	-561	-560	-385	-350	-280	-70	0	175	245
18	-1645	-1610	-1575	-1505	-1330	-1295	-1155	-945	-841	-840	-736	-735	-560	-525	-455	-245	-175	0	70
19	-1715	-1680	-1645	-1575	-1400	-1365	-1225	-1015	-911	-910	-806	-805	-630	-595	-525	-315	-245	-70	0

*Temporal baselines are calculated by the acquisition time of the master image minus that of the slave image. Thus, negative temporal baselines exist.

Table. 2. Doppler centroid frequency difference statistics of interferograms (unit: HZ)

image	1	2	3	4	5	6	7	8	9	10	11	12	13	14	15	16	17	18	19
1	0	-40	-13	-12	-64	6	59	-5	282	91	250	17	25	-23	63	-44	-15	313	157
2	40	0	27	28	-23	47	99	35	323	131	290	57	65	17	103	4	26	354	198
3	13	-27	0	1	-50	20	72	8	296	104	263	30	38	-10	76	-31	-1	327	171
4	12	-28	-1	0	-52	18	71	7	294	103	262	29	37	-11	75	-32	-3	325	169
5	64	23	50	52	0	70	122	59	346	155	313	81	89	41	127	20	49	377	221
6	-6	-47	-20	-18	-70	0	52	-12	276	84	241	10	19	-29	57	-50	-21	307	151
7	-59	-99	-72	-71	-122	-52	0	-64	224	32	191	-42	-34	-82	4	-103	-73	255	99
8	5	-35	-8	-7	-59	12	64	0	288	96	255	22	30	-18	68	-39	-10	318	162
9	-282	-323	-296	-294	-346	-276	-224	-288	0	-192	-33	-266	-256	-305	-219	-326	-297	31	-125
10	-91	-131	-104	-103	-155	-84	-32	-96	192	0	159	-73	-66	-114	-28	-135	-105	222	67
11	-250	-290	-263	-262	-313	-241	-191	-255	33	-159	0	-232	-225	-272	-186	-293	-264	64	-92
12	-17	-57	-30	-29	-81	-10	42	-22	266	73	232	0	8	-40	-3	64	288	297	141
13	-25	-65	-38	-37	-89	-19	34	-30	256	66	225	-8	0	-48	38	-69	-40	288	132
14	23	-17	10	11	-41	29	82	18	305	114	272	40	48	0	86	-21	8	336	97
15	-63	-103	-76	-75	-127	-57	-4	-68	219	28	186	3	-38	-86	0	-107	-78	250	94
16	44	-4	31	32	-20	50	103	39	326	135	293	61	69	21	107	0	29	357	201
17	15	-26	1	3	-49	21	73	10	297	105	264	31	40	-8	78	-29	0	328	172
18	-313	-354	-327	-325	-377	-307	-255	-318	-31	-222	-64	-296	-288	-336	-250	-357	-328	0	-156
19	-157	-198	-171	-169	-221	-151	-99	-162	125	-67	92	-141	-180	-97	-94	-201	-172	156	0

*Doppler centroid frequency differences are calculated by the value of the master image minus that of the slave image. Thus, negative Doppler centroid frequency differences exist.

Table. 3. Effective spatial baseline statistics of interferograms (unit: meter)

image	1	2	3	4	5	6	7	8	9	10	11	12	13	14	15	16	17	18	19
1	0	446	151	17	124	86	673	-287	217	176	179	96	302	56	93	160	384	393	399
2	-446	0	-295	-429	-322	-360	227	-733	-229	-270	-267	-350	-144	-390	-353	-286	-62	-53	-47
3	-151	295	0	-134	-27	-65	522	-438	66	25	28	-55	151	-95	-58	9	233	242	248
4	-17	429	134	0	107	69	656	-304	200	159	162	79	285	39	76	143	367	376	382
5	-124	322	27	-107	0	-38	549	-411	93	52	55	-28	178	-68	-31	36	260	269	275
6	-86	360	65	-69	38	0	587	-373	131	90	93	10	216	-30	7	74	298	307	313
7	-673	-227	-522	-656	-549	-587	0	-960	-456	-497	-494	-577	-371	-617	-580	-513	-289	-280	-274
8	287	733	438	304	411	373	960	0	504	463	466	383	589	343	380	447	671	680	686
9	-217	229	-66	-200	-93	-131	456	-504	0	-41	-38	-121	85	-161	-124	-57	167	176	182
10	-176	270	-25	-159	-52	-90	497	-463	41	0	3	-80	126	-120	-83	-16	208	217	223
11	-179	267	-28	-162	-55	-93	494	-466	38	-3	0	83	123	-123	-86	-19	205	214	220
12	-96	350	55	-79	28	-10	577	-383	121	80	83	0	206	-40	-3	64	288	297	303
13	-302	144	-151	-285	-178	-216	371	-589	-85	-126	-123	-206	0	-246	-209	-142	82	91	97
14	-56	390	95	-39	68	30	617	-343	161	120	123	40	246	0	37	104	328	337	343
15	-93	353	58	-76	31	-7	580	-380	124	83	86	3	209	-37	0	67	291	300	306
16	-160	286	-9	-143	-36	-74	513	-447	-57	16	19	-64	142	-104	-67	0	224	233	239
17	-384	62	-233	-367	-260	-298	289	-671	-167	-208	-205	-288	-82	-328	-291	-224	0	9	15
18	-393	53	-242	-376	-269	-307	280	-680	-176	-217	-214	-297	-91	-337	-300	-233	-9	0	6
19	-399	47	-248	-382	-275	-313	274	-686	-182	-223	-806	-220	-303	-97	-343	-306	-239	-15	-60

*Effective spatial baselines are calculated by the perpendicular baseline of the master image minus that of the slave image. Thus, negative effective spatial baselines exist.

Following the model of comprehensive correlation coefficients by Chen[13, 20], the coefficients are assigned with 1 in the current study to select exponential values without significantly affecting the result[15]. The result with maximum sum of weights, minimum sum of three baselines, and integrated correlation coefficient are shown in the following diagram.

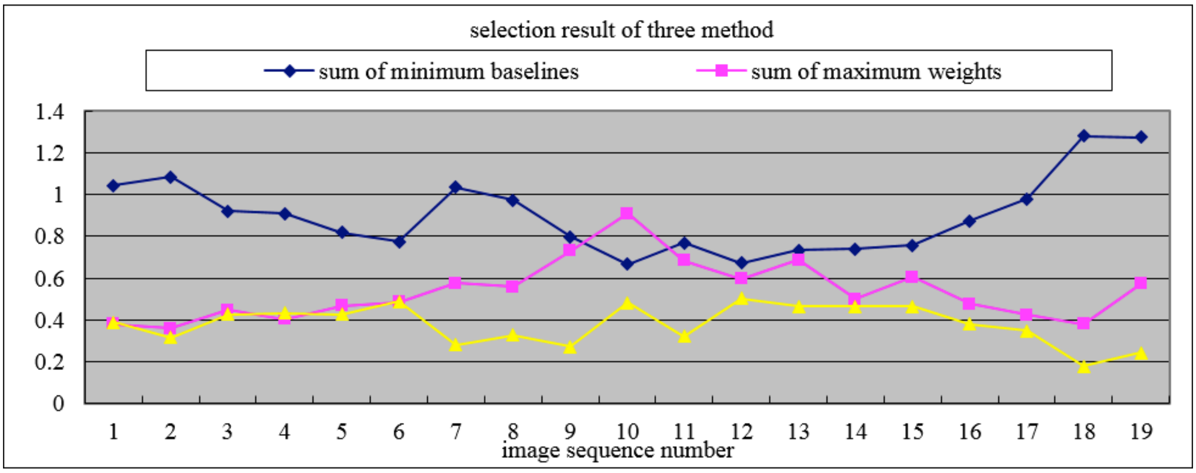

Fig. 2. Result with maximum sum of weights, minimum sum of three baselines, and integrated correlation coefficient

As shown in Figure 2, the selection result computed by the maximum sum of the weights model is considerably better than that by the integrated correlation coefficient model. Datasets 10, 9, and 13 are the top three images calculated by the former model.

To illustrate the situation of the three components of the maximum sum of weights model, the three components are listed separately in Figure 3.

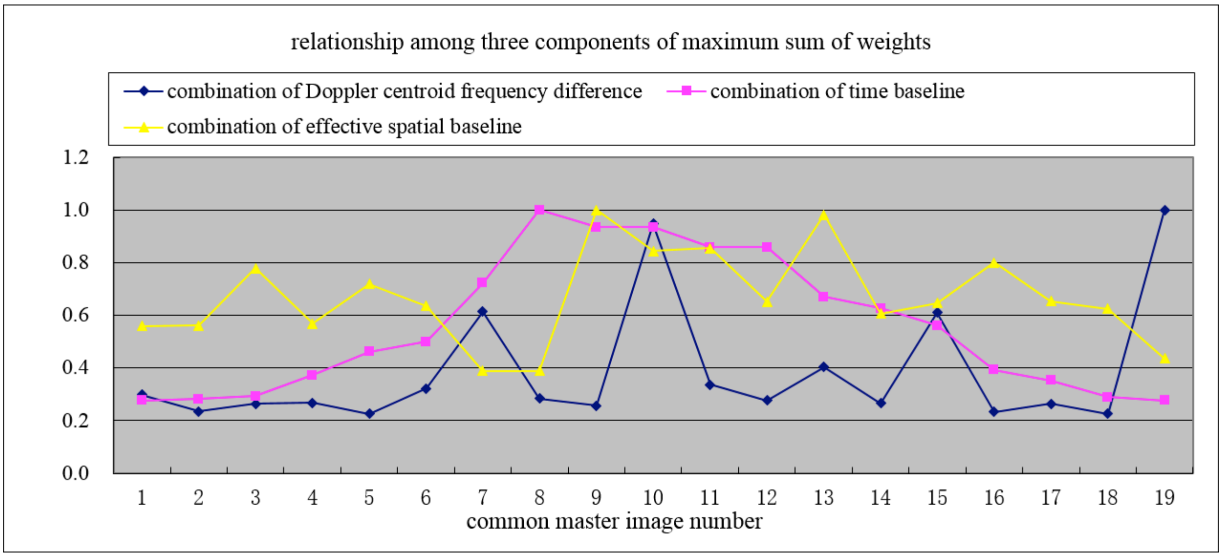

Fig. 3. Relationship among three components of maximum sum of weights

The weight of each component of maximum sum of weights is shown in Figure 3. Clearly, the line chart of temporal baseline exerts a significant effect, especially the points near the middle place. The characteristics of the weights of effective spatial baseline combination and Doppler centroid frequency difference combination are not evident.

The calculated results of the integrated correlation coefficient in the top three combinations of serial numbers are groups 12, 6, and 10. The results of the minimum sum of the baseline model in the top three combinations of serial numbers are combinations 12, 10, and 13[13], and those of the maximum sum of the weights model in the top three combinations of serial numbers are combinations 10, 9, and 13. The selection by these models is shown in Table 4.

Table. 4. Optimum common master image selected by three models

model \ choice	first choice	Second choice	Third choice
integrated correlation coefficient model	12	6	10
minimum sum of baselines model	12	10	13
Maximum sum of weights model	10	9	13

Groups 10 and 12 are for optimum selection. For comparison, temporal baseline combination, effective spatial combination, and differential Doppler centroid combination in groups 10 and 12 are analyzed. The results are shown in Figure 4.

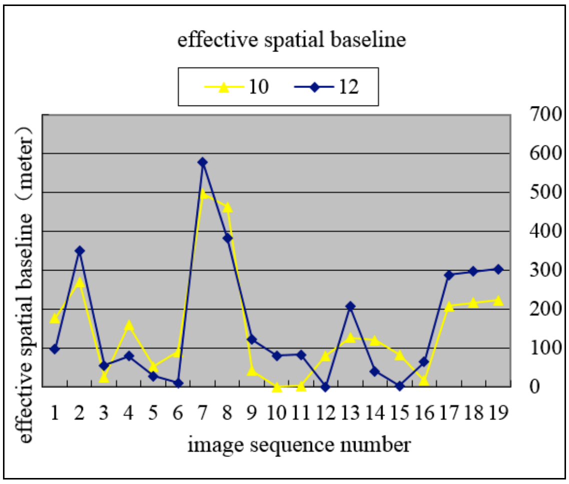

(a)

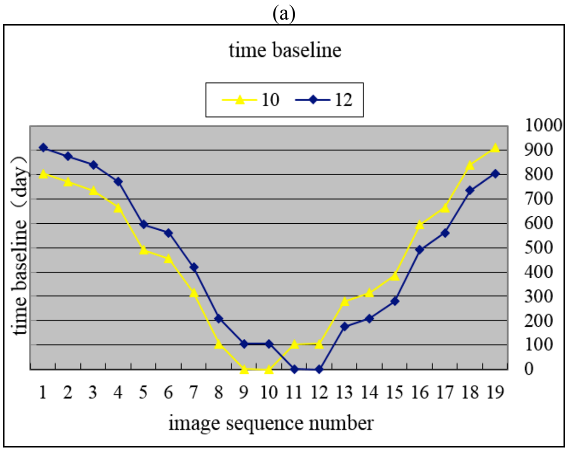

(b)

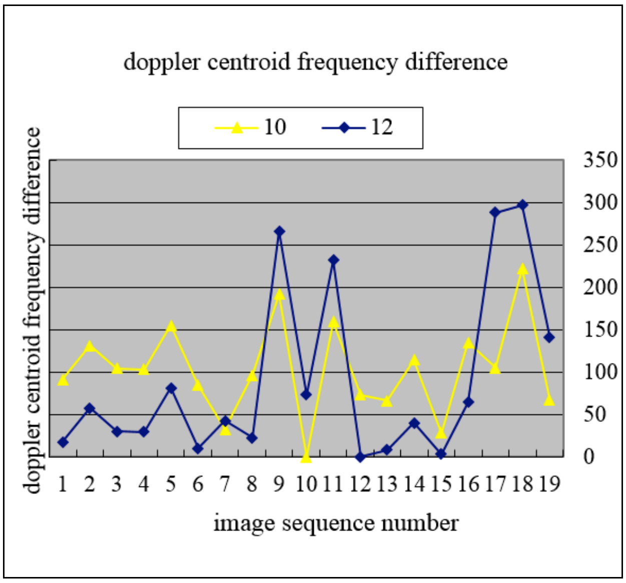

(c)

Fig. 4. Comparison among effective spatial baselines, temporal baselines, and Doppler centroid frequency differences of groups 10 and 12 SAR images

Comparison results of combinations 10 and 12 show that in the effective spatial baseline (Figure 4a), dataset 10 is better than dataset 12 in maximum and stability values. No obvious distinctions are found between datasets 10 and 12 in the temporal baseline (Figure 4b). Group 10 performs considerably better in maximum value compared with group 12. Furthermore, the maximum value of 10 is obviously less than that of 12 in the combination of Doppler centroid difference. The values of Doppler centroid model in images from 1 to 8 are a little large.

The quantitative analysis of the statistical information in combinations 10 and 12 is listed in Table 5. Only the value of Doppler centroid frequency differences in combination 10 is larger than that in combination 12, and the rest is considerably better. This result can be attributed to the fact that combination 10 is more optimized than combination 12. Therefore, group 10 can be prioritized in the selection of the common master image.

Table. 5. Baseline statistics of combinations 10 and 12

Influencing factors	Image number	max	min	Standard deviation
Temporal Baseline	10	910	449	299
	12	910	455	312
Doppler centroid frequency difference	10	222	103	55
	12	297	89	102
Effective spatial baseline	10	497	149	141
	12	577	161	161

The second and third options in the integrated correlation coefficient model are combinations 6 and 10, respectively. A reasonable combination is selected by comparing the temporal baseline combination, effective spatial baseline combination, and Doppler centroid difference combination in groups 6 and 10. The results are shown in Figure 5.

Comparison of datasets 6 and 10 shows that (Figure 5a) combination 10 is superior in the effective spatial baseline because its maximum and stability values are better than those of combination 6. The maximum and average values of 10 are also better than those of 6 in the temporal baseline combination (Figure 5b). In the Doppler centroid difference combination (Figure 5c), the maximum value of 10 is relatively stable and is significantly less than that of combination 6.

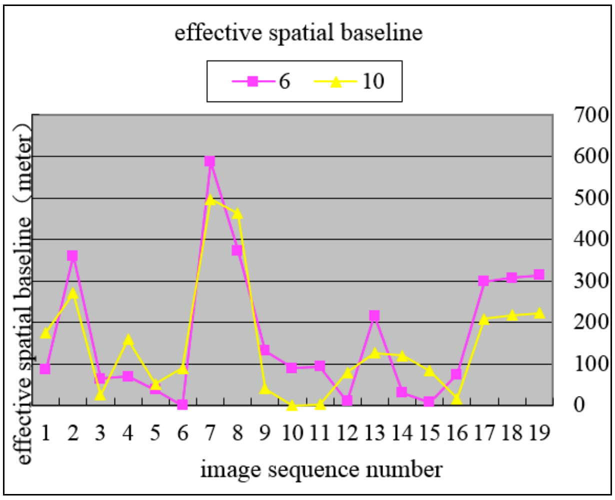

(a)

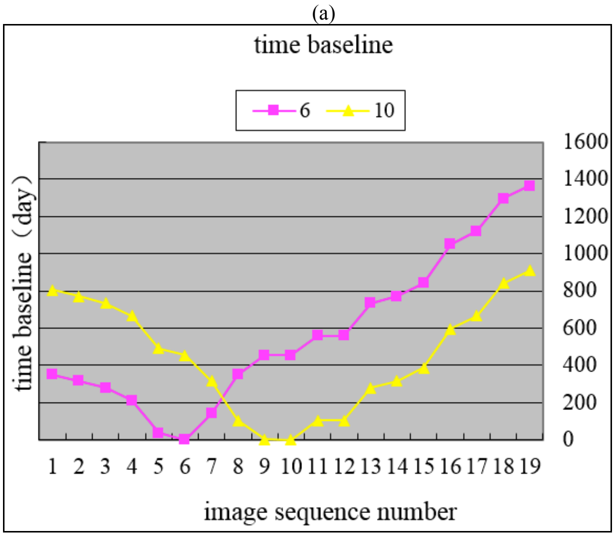

(b)

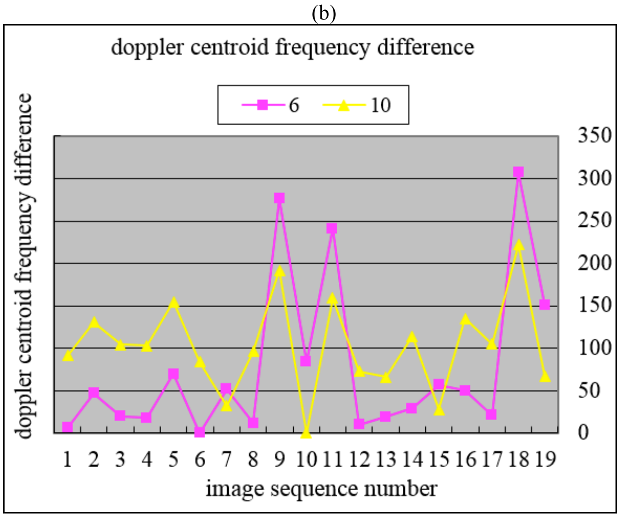

(c)

Fig. 5. Comparison among effective spatial baselines, temporal baselines, and Doppler centroid frequency differences of groups 6 and 10 SAR images

For the quantitative analysis, statistical information of the two combinations is listed in Table 6. The values of combination 10 are better than those of combination 6. Therefore, dataset 10 is a good choice for selecting the common master image.

Table. 6. Baseline statistics of combinations 6 and 10

Influencing factors	Image number	max	min	Standard deviation
Temporal baseline	6 10	1365 910	572 449	410 299
Doppler centroid frequency difference	6 10	307 222	77 103	95 55
Effective spatial baseline	6 10	587 497	165 149	162 141

To determine the characteristics in the maximum sum of weights model, the first and second alternatives in datasets 10 and 9 are compared. The illustrations are shown in Figure 6.

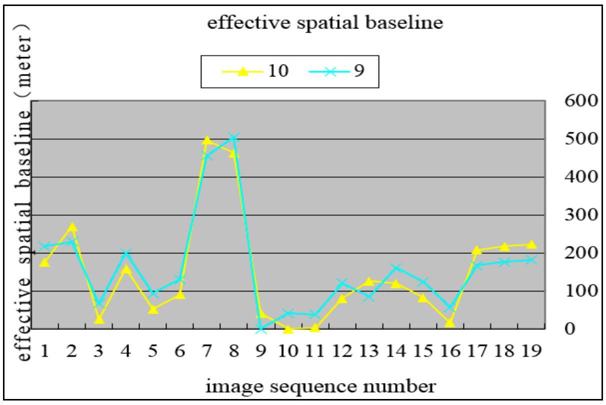

(a)

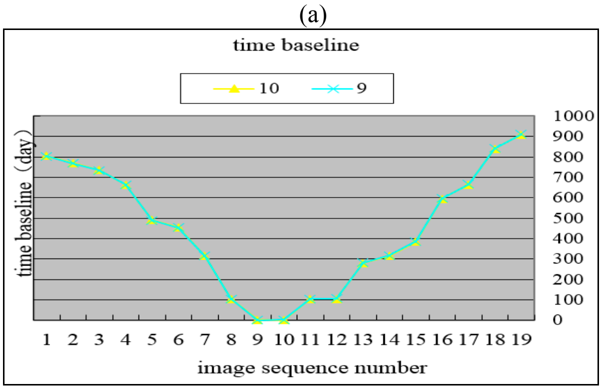

(b)

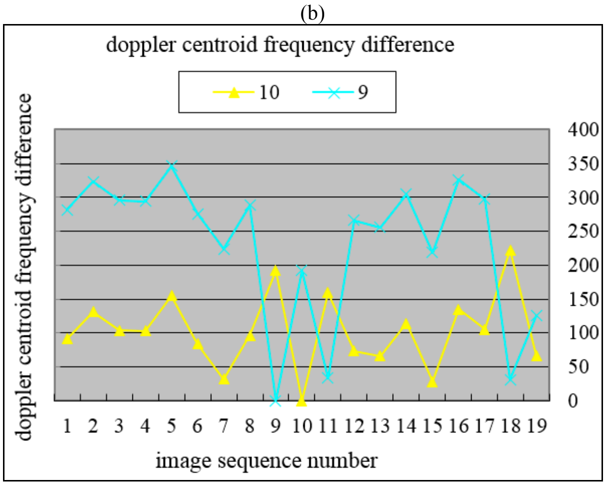

(c)

Fig. 6. Comparison among effective spatial baselines, temporal baselines, and Doppler centroid frequency differences of 9 and 10 SAR images

Comparison of combinations 9 and 10 shows that in the temporal baseline combination (Figure 6a) and effective spatial baseline combination (Figure 6b), combinations 9 and 10 are nearly the same. Only the instability and volatility of combination 9 are found for the Doppler centroid frequency difference (Figure 6c). Therefore, combination 10 is more reasonable than combination 9.

Statistical data of combinations 9 and 10 are listed in Table 7.

Table. 7. Baseline statistics of combinations 9 and 10

Influencing factors	Image number	max	min	Standard deviation
Temporal baseline	9 10	911 910	449 449	299 299
Doppler centroid frequency difference	9 10	346 222	230 103	106 55
Effective spatial baseline	9 10	504 497	160 149	130 141

Clearly, most statistical data of combination 10 are better than those of combination 9.

5 Conclusion

In PS-DINSAR technology, appropriate selection of common master image can improve the quality of the interferograms. An idea based on fixed weights of observed values in the surveying adjustment was used in this study to select the common master image. The temporal baseline combination, effective spatial baseline combination, and Doppler centroid frequency difference combination were regarded separately as equal-precision observations. The RMSE and weight of observations were calculated. The best interferogram series could then be selected by the maximum sum of weights. The following conclusions could be drawn.

(1) The proposed method based on fixed weights of observed values in the surveying adjustment is suitable for selecting the common master image. Using the maximum sum of weights to select the common master image is more stable than using other methods. The results are also superior in the aspect of statistical theorem.

(2) The temporal baseline, effective spatial baseline, and Doppler centroid frequency difference are regarded as observed values in individual groups. The weights of each observed group are calculated, and the influence of each factor on the ultimate interferogram result is considered.

(3) Three main factors, namely, temporal baseline, effective spatial baseline, and Doppler centroid frequency difference, are considered in the model. The methods are simple in calculation and convenient for batch processing of image data.

In view of the imaging feature of data, the proposed method can be used for optimal selection of the common master image. However, datasets from various remote sensing platforms present different characteristics. Thus, further research is needed to ensure the application of the technique on datasets from various platforms.

Acknowledgements

This work was supported by the Science and Technology Research Project of Jiangxi Provincial Education Department (Grant No. GJJ170468), Key Laboratory for Digital Land and Resources of Jiangxi Province East China University of Technology (Grant No. DLLJ201717), Jiangxi Province Education Science "13th Five-Year" Program (Grant No. 17YB070, 17YB079, GJJ150557 and NRE508).

References

1. Ferretti, A., Rocca, F., "Permanent Scatters in SAR interferometry". *IEEE Transactions on Geoscience and Remote Sensing,* 39(1), 2001, pp.8-20.
2. Ferretti, A., "InSAR permanent scatterer analysis reveals ups and downs in San Francisco Bay area". *Transactions American Geophysical Union*, 85(34), 2004, pp.317.
3. Maghsoudi, Y., van der Meer, F., Hecker, C., Perissin, D., Saepuloh, A., "Using PS-InSAR to detect surface deformation in geothermal areas of West Java in Indonesia". *International Journal of Applied Earth Observation and Geoinformation*, 64(Supplement C), 2018, pp.386-396.
4. Rosi, A., Tofani, V., Tanteri, L., Tacconi Stefanelli, C., Agostini, A., Catani, F., Casagli, N., "The new landslide inventory of Tuscany (Italy) updated with PS-InSAR: geomorphological features and landslide distribution". *Landslides*, (5), 2017, pp.1-15.
5. Armaş, I., Mendes, D. A., Popa, R. G., Gheorghe, M., Popovici, D., "Long-term ground deformation patterns of Bucharest using multi-temporal InSAR and multivariate dynamic analyses: a possible transpressional system". *Scientific Reports*, 7, 2017, pp.437-462.
6. Amato, V., Aucelli, P. P. C., Bellucci S., E., Cesarano, M., Incontri, P., Pappone, G., Valente, E., Vilardo, G., "Multidisciplinary approach for fault detection: integration of PS-InSAR, geomorphological, stratigraphic and structural data in the Venafro intermontane basin (Central-Southern Apennines, Italy)". *Geomorphology*, 283, 2017, pp.80-101.
7. Fokker, P. A., Wassing, B. B. T., van Leijen, F. J., Hanssen, R. F., Nieuwland, D. A., "Application of an ensemble smoother with multiple data assimilation to the Bergermeer gas field, using PS-InSAR". *Geomechanics for Energy and the Environment,* (5), 2016, pp.16-28.
8. Ciampalini, A., Raspini, F., Frodella, W., Bardi, F., Bianchini, S., Moretti, S., "The effectiveness of high-resolution LiDAR data combined with PSInSAR data in landslide study". *Landslides*, 13(2), 2016, pp.399-410.
9. Peduto, D., Cascini, L., Arena, L., Ferlisi, S., Fornaro, G., Reale, D., "A general framework and related procedures for multiscale analyses of DInSAR data in subsiding urban areas". *ISPRS Journal of Photogrammetry and Remote Sensing,* 105, 2015, pp.186-210.
10. Notti, D., Calò, F., Cigna, F., Manunta, M., Herrera, G., Berti, M., Meisina, C., Tapete, D., Zucca, F., "A user-oriented methodology for DInSAR time series analysis and interpretation: Landslides and Subsidence Case Studies". *Pure and Applied Geophysics*, 172(11), 2015, pp.3081-3105.
11. Kiseleva, E., Mikhailov, V., Smolyaninova, E., Dmitriev, P., Golubev, V., Timoshkina, E., Hooper, A., Samiei, E., S., Hanssen, R., "PS-InSAR monitoring of landslide activity in the Black Sea Coast of thecaucasus". *Procedia Technology*, 16(Supplement C), 2014, pp.404-413.
12. Perrone, G., Morelli, M., Piana, F., Fioraso, G., Nicolò, G., Mallen, L., Cadoppi, P., Balestro, G., Tallone, S., "Current tectonic activity and differential uplift along the Cottian Alps/Po Plain boundary (NW Italy) as derived by PS-InSAR data". *Journal of Geodynamics*, 66, 2013, pp.65-78.
13. Hooper, A., Zebker, H. A., Segall, P., "A new method for measuring deformation on volcanoes and other natural terrains using InSAR persistent scatterers". *Geophysical research letters*, 31(L23611), 2004, pp.1-5.
14. Kampes, B. M., Hassen, R. F., "Ambiguity resolution for permanent scatterer interferometry". *IEEE Transactions on Geoscience and Remote Sensing,* 42(11), 2004, pp.2446-2453.
15. Tao, Q. X., Liu, G. l., "A new method to optimize and select common master images in PS InSAR". *Geomatics and Information Science of Wuhan University*, 36(12), 2011, pp.1456-1460.
16. Kampes, B. M. "*Displacement parameter estimation using Permanent Scatterer Interferometry*" Master thesis of Delft University of technology: Delft, USA, 2005, pp.18-32.
17. Chang, C. P., Yen, J. Y., Hooper, A., Chou, F. M., Chen, Y.A., Hou, C. S., Hung, W. C., Lin, M. S., "Monitoring of surface deformation in Northern Taiwan using DInSAR and PSInSAR techniques" *terrestrial atmospheric and oceanic sciences*, 21(3), 2010, pp447-461.
18. Zebker, H. A., Villasenor, J., "Decorrelation in Interferometric Radar Echoes". *IEEE Transactions on Geoscience and Remote Sensing Remote Sensing,* 30(5), 1992, pp.950-959.
19. Zhang, H., Zeng, Q., Liu, Y., "The optimum selection of common master image for series of defferential SAR processing to estimate long and slow ground deformation". In: *Geoscience and Remote Sensing Symposium, 2005. IGARSS '05*. Seoul, South Korea: IEEE, 2005, pp.4586-4589.
20. Chen, Q., Ding, X., Liu, G., "Method for optimum selection of common master acquisition for PS-DInSAR". *Acta Geodaetica et Cartographica Sinica,* 36(4), 2007, pp.395-399.
21. Wang, Z., Zhang, J. Q., "A method for selecting common master images in PS-InSAR". *Remote Sensing Information*, (1), 2013, pp.49-53.
22. Luo, H. B., He, X. F., "Method of time series differential interferogram common master image selection for PS-DInSAR". *Journal of Hehai University(Natural Sciences)*, (3), 2011, pp.344-347.
23. Pan, B., Shu, M., "Cluster analysis for selection of time series interferometric SAR imagery". *Journal of Applied Sciences*, 28(5), 2010, pp.501-506.
24. Liu, L. M., Gong, L. H., Yu, J., Chen, P. P., "A new optimization selection method of common master image for PS-InSAR interferometry". *Geomatics and Information Science of Wuhan University,* 12, 2015, pp.1594-1599+1612.
25. Long, S. C., Liu, J. G., Li, T., Tang, C. H., "Method for optimum selection of common master acquisition for PS-DInSAR fusing GPS data". *Journal of Tongji University(Natural Science)*, 38(3), 2010, pp.453-458.